AMERICAN SOCIETY FOR MICROBIOLOGY | mBio®

RESEARCH ARTICLE

Lineages Derived from *Cryptococcus neoformans* Type Strain H99 Support a Link between the Capacity to Be Pleomorphic and Virulence

Kenya E. Fernandes,[a] James A. Fraser,[b] Dee A. Carter[a,c]

[a]School of Life and Environmental Sciences, University of Sydney, Sydney, NSW, Australia
[b]School of Chemistry and Molecular Biosciences, Australian Infectious Diseases Research Centre, The University of Queensland, St. Lucia, QLD, Australia
[c]Sydney Institute for Infectious Diseases, University of Sydney, Sydney, NSW, Australia

ABSTRACT The pathogenic yeast *Cryptococcus neoformans* causes nearly 200,000 deaths annually in immunocompromised individuals. *Cryptococcus* cells can undergo substantial morphological change during mammalian infection, including increased capsule and cell size, the release of shed capsule, and the production of titan (>10 μm), micro (<2 μm)-, and irregular cells. We examined phenotypic variation under conditions designed to simulate *in vivo* stress in a collection of nine lineages derived from the *C. neoformans* type strain H99. These lineages are highly genetically similar but have a range of virulence levels. Strains from hypervirulent lineages had a larger average capsule size, greater variation in cell size, and an increased production of microcells and shed capsule. We tested whether disruption of *SGF29*, which encodes a component of the SAGA histone acetylation complex that has previously been implicated in the hypervirulence of some lineages, also has a role in the production of morphological variants. Deletion of *SGF29* in a lineage with intermediate virulence substantially increased its production of microcells and released capsule, consistent with a switch to hypervirulence. We further examined *SGF29* in a set of 52 clinical isolates and found loss-of-function mutations were significantly correlated with patient death. Expansion of a TA repeat in the second intron of *SGF29* was positively correlated with cell and capsule size, suggesting it also affects Sgf29 function. This study extends the evidence for a link between pleomorphism and virulence in *Cryptococcus*, with a likely role for epigenetic mechanisms mediated by SAGA-induced histone acetylation.

IMPORTANCE Cryptococcosis is a devastating cause of death and disease worldwide. During infection, *Cryptococcus* cells can undergo substantial changes to their size and shape. In this study, we used a collection of *C. neoformans* strains that are highly genetically similar but possess differing levels of virulence to investigate how morphological variation aligns with virulence. We found hypervirulent strains on average had larger capsules and greater variation in cell size and produced more microcells and shed capsule. These hypervirulent strains possessed a mutation in *SGF29*, which encodes a component of the SAGA complex involved in epigenetic regulation. Analysis of the *SGF29* gene in a set of clinical isolates found strains with loss-of-function mutations were associated with higher patient death rates. The capacity to vary appears to be linked with virulence in *Cryptococcus*, and this can occur in the absence of genetic variation via epigenetic mechanisms.

KEYWORDS *Cryptococcus neoformans*, SAGA complex, giant cells, microcells, pleomorphism, virulence

Cryptococcus neoformans is an encapsulated yeast pathogen that primarily infects immunocompromised people and can cause severe meningoencephalitis (1). Despite progress in reducing the incidence and burden of disease through improved

Editor Yong-Sun Bahn, Yonsei University

Address correspondence to Dee A. Carter, dee.carter@sydney.edu.au.

The authors declare no conflict of interest.

This article is a direct contribution from Dee A. Carter, a Fellow of the American Academy of Microbiology, who arranged for and secured reviews by Robin May, University of Birmingham, and Kirsten Nielsen, University of Minnesota Medical School.

Received 7 February 2022
Accepted 11 February 2022
Published 8 March 2022

diagnostic strategies and access to antiretroviral therapy, the mortality rate associated with cryptococcosis still remains unacceptably high (2). In addition to a paucity of effective and widely available antifungal drugs (3), there is incomplete knowledge of the interplay between pathogen and host with which to inform clinical management (1). Cryptococcosis can be associated with a range of clinical presentations and outcomes, and this is determined in part by variations in the infecting strain (3). During mammalian infection, genetically identical *Cryptococcus* cells can undergo substantial phenotypic variation, including the production of titan, micro-, and irregular cell variants, a dramatic increase in capsule size, and the shedding of capsule (4). These changes to the size and shape of cells are frequently observed in clinical samples; however, relatively little is known about the full variety of morphologies that cryptococcal cells can produce and how this affects their pathogenicity.

Previously, we investigated phenotypic variation in a collection of 70 isolates from HIV/AIDS patients from Botswana with cryptococcosis and found significant correlations between phenotypic and clinical data (5). In particular, the combined presence of giant cells (which we defined as cells that are in the size range of titan cells [$>$15 μm] but cannot be definitively described as titan cells, as polyploidy and increased cell wall chitin [6, 7] have not been determined), microcells ($\leq$1 μm) and shed capsule, while rare, was positively correlated with patient death, indicating that the capacity for variation plays a role in virulence. While interesting correlations were uncovered by this study, it was limited to being mostly descriptive, with the high level of diversity present in both the cryptococcal isolates and host populations confounding efforts to tease apart cause and effect.

Cryptococcus neoformans strain H99 was first isolated in 1978 and has since become the most widely used *C. neoformans* reference strain globally. During storage, passage, and subculture in various labs around the world, distinct H99 lineages have arisen with various levels of virulence (Fig. 1A) (8). Complete sequencing of strains representing these lineages has revealed a small number of unique mutations among them. Notably, the hypervirulent H99L lineage strains have a 734-bp deletion in the gene encoding Sgf29, a component of the SAGA histone acetylation complex. This complex is involved in controlling gene transcription through remodeling chromatin structure, and its loss has been shown to lead to a reduction in histone H3K9 acetylation across the genome (9). In H99L and its derivatives, the disruption of Sgf29 has been implicated in the switch to the hypervirulent phenotype, and Sgf29 loss-of-function mutations have been identified in clinical isolates (9). Additionally, a group of less virulent H99 lineages possesses a mutation in *LMP1* that compromises fecundity and virulence (8).

This set of very closely related H99 strains comprises a valuable resource for determining a link between virulence and phenotype in a background of high genetic similarity. Here, we examined variation in capsule and cell size in this strain set under *in vitro* conditions designed to simulate *in vivo* stress and provide evidence that the capacity for phenotypic variation is associated with increased virulence in these strains. We determined growth characteristics and antifungal susceptibility and confirmed that, in most respects, the strains were very similar, although hypervirulent strains showed slightly increased susceptibility to some drugs. Finally, we investigated the impact of mutations in *SGF29* on strains in the H99 derivative set and in the set of clinical isolates from Botswana that was investigated in our prior work.

RESULTS

H99 derivative strains display expected virulence and growth dynamics. The relationship between the nine H99 lineage strains used in this study is shown in Fig. 1A and B. H99O is believed to be one of the closest remaining relatives of the original H99 strain and is considered to have intermediate virulence. Hypervirulent strains H99L and H99F possess the 734-bp deletion in the gene encoding Sgf29 that appears to play a role in conferring the hypervirulent phenotype (9). The remaining hypervirulent strain H99S does not possess this mutation and is theorized to have acquired

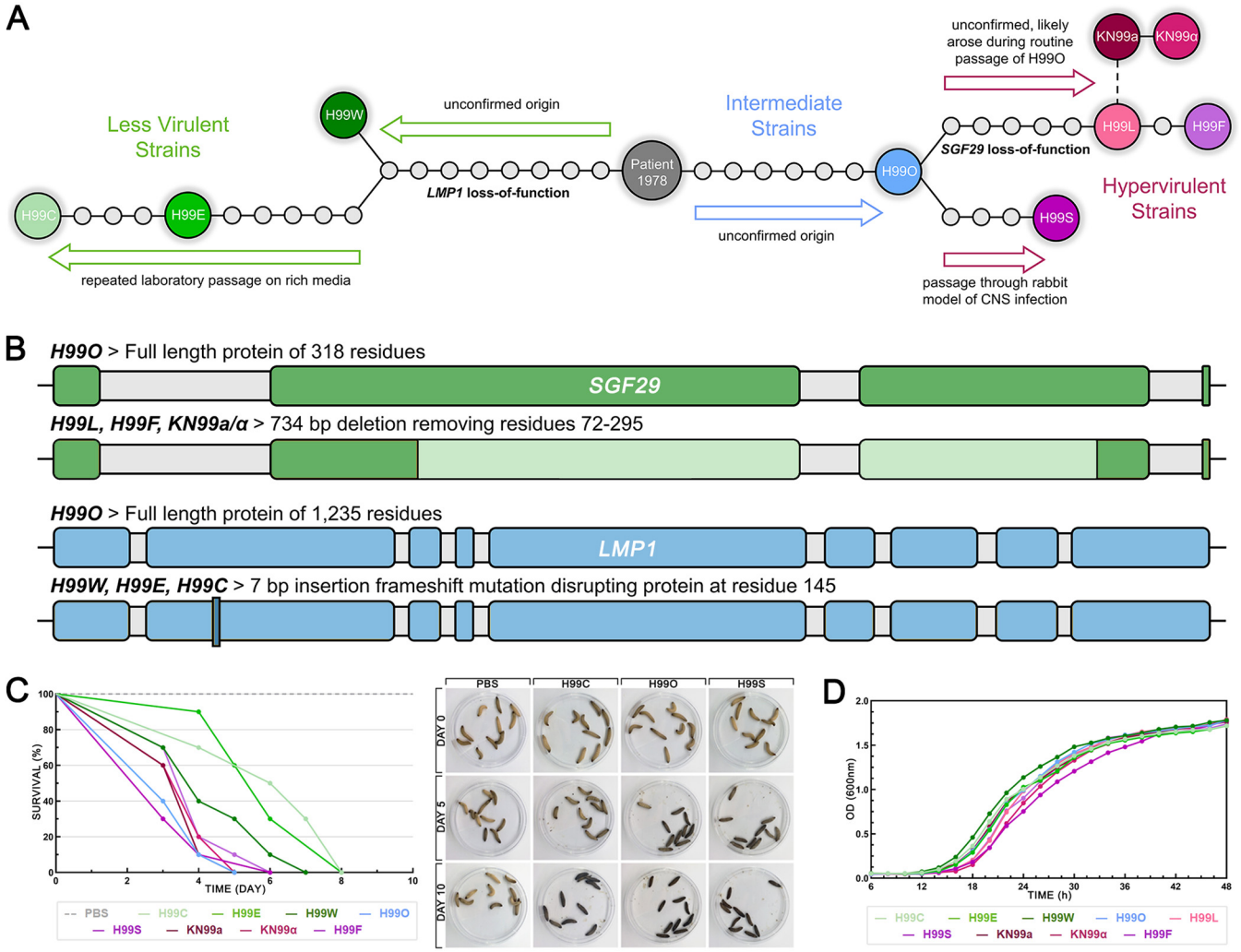

FIG 1 Origins of the *C. neoformans* H99 strains used in this study and their comparative virulence and growth dynamics. (A) The relationship between the H99 derivative strains used in this study. Mutations separating strains are shown by circles, and known or hypothesized directions of evolution are shown by arrows. Figure adapted from Arras et al. (9). CNS, central nervous system. (B) Diagram of the *SGF29* and *LMP1* genes showing disruptions found in some H99 derivative strains. Lighter-colored sections indicate areas of deletion, darker-colored sections indicate areas of insertion. Gray shading indicates introns. (C) Survival of *G. mellonella* larvae infected with an inoculum of 10^8 cells of each H99 strain or mock infected with PBS over 10 days; $n = 10$ for each treatment group. The left panel shows a representative survival plot (one of two independent replicates that gave similar results); the right panel shows photographs of representative larvae at days 0, 5, and 10 that had been mock infected (PBS) or infected with a less virulent (H99C), intermediate (H99O), or hypervirulent (H99S) strain. Treatment groups were compared by log rank test; H99C ($P \leq 0.017$) and H99E ($P \leq 0.019$) survived significantly longer than H99O, H99S, H99L, KN99**a**, KN99α, and H99F. (D) Growth curves of H99 strains incubated at 30°C with 180-rpm shaking averaged across three independent replicates, showing no substantial differences between strains.

hypervirulence in an independent manner (9). H99W, H99E, and H99C are the less virulent strains and possess the mutation in *LMP1* (8). Two additional closely related strains are included in the set: the congenic mating type pair KN99**a** and KN99α. These strains were created through repeat backcrossing between H99F and an unrelated *MAT***a** mating type isolate (10) and also display hypervirulence.

On receipt of the strains, we tested their virulence in *Galleria mellonella* (wax moth) larvae to confirm that they were behaving as expected (Fig. 1C). Larvae infected with less virulent strains H99C, H99E, and H99W survived 1 to 3 days longer than larvae infected with intermediate or hypervirulent strains, with H99C ($P \leq 0.017$) and H99E ($P \leq 0.019$) reaching significance against H99O, H99S, H99L, KN99**a**, KN99α, and H99F. These results were consistent with those previously obtained using the *G. mellonella* model (8). Analysis of the growth dynamics of strains under standard growth conditions (Sabouraud dextrose broth [SDB] at 30°C) over 48 h found no substantial difference among them, indicating that all strains were healthy and capable of similar,

TABLE 1 Strains used in this study with details of cell and capsule size, production of variant phenotypes and antifungal susceptibilities[a]

	Cell diam[d] (μm)		Capsule thickness[d] (μm)		Irregular	Frequency of[b]:				MIC[c] (μg/mL)					
Strain	Mean	SD or variance	Mean	SD or variance	cells[b] (%)	Giant cells	Microcells	Released capsule	Clustered capsule	AMB	NYS	FLC	ITC	VRC	5FC
Less virulent															
H99C	5.31	0.79	2.19	0.70	<5	–	–	–	+	0.5	4	4	0.25	0.125	8
H99E	5.64	0.84	2.27	0.73	<5	+	–	+	–	0.5	4	4	0.25	0.125	8
H99W	5.75	0.75	1.71	0.68	<5	–	–	+	+	0.5	4	4	0.25	0.125	8
All less virulent strains	5.57	**0.03**	2.06	**0.06**	**100**	**33**	**0**	**67**	**67**	**0.5**	**4**	**4**	**0.25**	**0.125**	**8**
Intermediate virulence															
H99O	5.87	1.01	3.30	0.88	<5	+	+	+	+	0.5	4	4	0.25	0.125	4
Hypervirulent															
H99S	5.86	1.21	3.07	0.77	<5	–	+	++	+ ++	0.5	4	2	0.125	0.063	4
H99L	5.65	1.37	3.33	0.76	<5	–	+	++	+++	0.5	4	4	0.25	0.125	4
KN99a	4.72	1.18	3.02	0.85	<10	–	+++	+++	+	0.5	4	1	0.125	0.031	4
KN99α	4.75	1.21	2.90	0.73	<10	–	+++	+++	++	0.5	4	1	0.125	0.063	4
H99F	5.69	1.48	2.96	0.83	<5	–	++	++	+++	0.5	4	4	0.125	0.125	4
All hypervirulent strains	5.33	**0.24**	3.06	**0.02**	**100**	**0**	**100**	**100**	**100**	**0.5**	**4**	**2**	**0.14**	**0.07**	**4**
H99O SGF29 Knockouts															
H99O.2	5.41	1.34	3.31	1.13	<5	–	+	+	+	0.5	4	4	0.25	0.125	4
H99OΔ	5.53	1.32	3.23	0.60	<5	–	++	++	++	0.5	4	4	0.25	0.125	4
H99OΔ+	5.26	1.79	3.32	1.49	<5	–	++	++	++	0.5	4	4	0.25	0.125	4
All H99O KO Strains	5.40	**0.01**	3.29	**0.00**	**100**	**0**	**100**	**100**	**100**	**0.5**	**4**	**4**	**0.25**	**0.125**	**4**
H99S SGF29 knockouts															
H99S.2	5.28	1.14	3.35	0.63	<5	–	+	+	++	0.5	4	2	0.125	0.063	4
H99SΔ	5.27	1.11	3.32	0.57	<5	–	+	+	++	0.5	4	4	0.25	0.125	4
H99SΔ+	5.56	1.16	3.14	0.69	<5	–	+	+	++	0.5	4	4	0.25	0.125	4
All H99S KO strains	5.37	**0.02**	3.27	**0.01**	**100**	**0**	**100**	**100**	**100**	**0.5**	**4**	**3.17**	**0.20**	**0.10**	**4**

[a]Giant, micro-, and irregular cells were excluded from calculations of cell diameter and capsule thickness.
[b]The relative frequency of each morphological variant is shown for individual strains; see Fig. 3A for scoring process. Values in boldface indicate percentage of strains with phenotype.
[c]AMB, amphotericin B; NYS, nystatin; FLC, fluconazole; ITC, itraconazole; VRC, voriconazole; 5FC, 5-fluorocytosine. Values in boldface are geomeans.
[d]Values in boldface are variance.

normal growth (Fig. 1D). Antifungal susceptibility to six commonly used antifungal drugs (amphotericin B [AMB], nystatin [NYS], fluconazole [FLC], itraconazole [ITC], voriconazole [VRC], and flucytosine [5FC]) found all strains were equally susceptible to polyene drugs AMB and NYS, while the hypervirulent strains H99S, KN99**a**, KN99α, and H99F had increased susceptibility to azole drugs FLC, ITC, and VRC, and less virulent strains were 2-fold less susceptible to 5FC (Table 1).

Hypervirulent strains produce cells with greater variation in size and larger capsules. Capsule thickness and cell body diameter were measured for 100 individual cells per strain after growth under capsule-inducing conditions (Dulbecco's modified Eagle medium [DMEM] with CO_2 at 37°C for 5 days) (Table 1, Fig. 2A and B). Figure 2C shows the microscopic morphology of typical cells from each strain. The capsule thickness of less virulent strains was, on average, approximately 50% less than that of intermediate and hypervirulent strains ($P < 0.0001$). Hypervirulent strain H99L and intermediate strain H99O had the largest average capsules, with H99L reaching significance against all other hypervirulent strains ($P \leq 0.0165$). F test analysis revealed that within the less virulent strains there was considerably less variation in capsule thickness, with H99W and H99C having significantly less variation than intermediate strain H99O ($P = 0.0145$ and $P = 0.0276$, respectively). For average cell body diameter, hypervirulent strains KN99**a** and KN99α were significantly smaller than all other intermediate and hypervirulent strains ($P < 0.0001$) as well as the less virulent strains ($P \leq 0.0002$). Intermediate strain H99O and hypervirulent strain H99S had the largest cell body diameters, while the remaining less virulent and hypervirulent strains ranked in the middle. Once again, there was much less variation in cell diameter in less virulent strains than intermediate strain H99O ($P \leq 0.0028$) and all hypervirulent strains ($P \leq 0.0001$). Hypervirulent strains displayed the most cell diameter variation in general, with significance reached against intermediate strain H99O by H99F ($P = 0.0002$) and H99L ($P = 0.0029$).

Hypervirulent strains produce morphological variants with higher frequency. Reports on the typical size of cryptococcal cells vary, but they are generally considered to be from 4 to 10 μm in diameter (11, 12). Cells substantially larger than average have previously been defined as titan/giant cells; however, the exact size definition has varied, including a cell body size of $>$10 μm, a cell body size of $>$15 μm, and total cell size, including capsule of $>$30 μm (13–16). Likewise, cells substantially smaller than average have previously been defined as microcells, typically defined as a cell body size of $<$1 μm (17). The current study found that following capsule induction, the average cell body size of H99 derivative strains ranged from 4.72 μm (KN99α) to 5.87 μm (H99O), with $>$90% of cells falling between 3 and 8 μm. Based on this, we have defined any cell with a cell body size of $>$10 μm as a giant cell and any cell with cell body size of $<$2 μm as a microcell, as these cell sizes were distinctly separate from average cells. The frequency with which these variant cell types were observed in each strain, along with the frequency of extracellular capsule seen either clustered tightly around groups of cells (clustered capsule) or released into the media (released capsule), is shown in Table 1 and Fig. 3. Elongated and irregularly shaped cells were also seen across all strains, but these comprised a small subset ($<$5%) of the total population of cells, except in KN99**a** and KN99α, where they were around twice as common ($<$10%) (Table 1).

Giant cells were observed very infrequently and in only two strains: H99E and H99O. Microcells were observed in all intermediate and hypervirulent strains and were particularly abundant in KN99**a** and KN99α but were absent from the less virulent strains. Released capsule and clustered capsule were similarly observed in all intermediate and hypervirulent strains. Unlike microcells, these were each present in two of the three less virulent strains; however, they were low in abundance. Clustered capsule was particularly abundant in hypervirulent strains H99S, H99L, and H99F, while released capsule was abundant in KN99**a** and KN99α. Overall, each of the hypervirulent strains were observed to produce three out of four of these variant phenotypes and with generally much higher frequency relative to intermediate and less virulent strains. Intermediate strain H99O

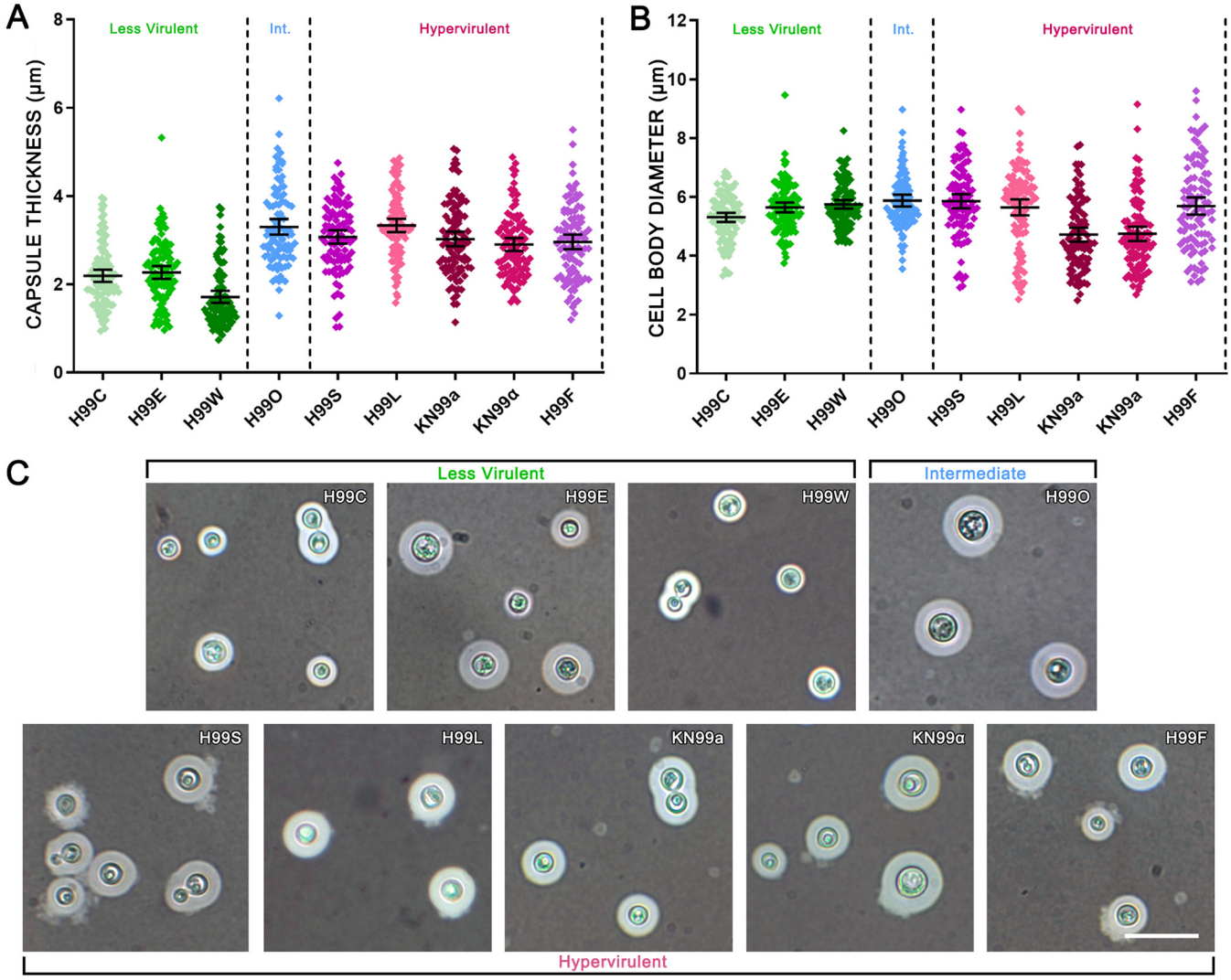

FIG 2 Less virulent H99 strains produce significantly smaller capsules following growth under capsule-inducing conditions. Capsule thickness (A) and cell body diameter (B) of 100 individual cells of each strain grown in DMEM with 5% CO_2 at 37°C for 5 days are shown. Strains were compared using two-tailed unpaired *t* tests with Welch's correction (significance described in Results). Error bars show the means ±95% confidence intervals. Int., intermediate. Giant, micro-, and irregular cells were excluded from this analysis. (C) India ink preparations of each strain showing variation in capsule and cell size. Scale bar, 15 μm.

produced all four variants but with lower relative frequency, while less virulent strains produced between one and two variants with similarly low frequency.

Electron microscopy reveals defined internal structures in the various cell types. Serial block-face scanning electron microscopy (SBF-SEM) was used to investigate the internal morphology of the giant, micro-, and irregular cells to confirm that they possess attributes of functional cells. SBF-SEM is a powerful imaging technique that generates serial images through a cell by repeated cutting, raising, and imaging of the sample block; however, the tradeoff is that due to electron charging it can have a reduction in resolution compared to transmission electron microscopy (TEM) (18). Figure S1A to D shows representative regular, giant, micro-, and irregular cells with slices taken at 10-nm intervals. The giant cell has a thicker cell wall (820 nm) than the regular cells (510 nm) and microcells (330 nm), while the cell wall of the irregular cell was particularly thin (260 nm). The giant cells also appeared to have numerous small vesicles. The internal structure of the micro- and irregular cells appeared very similar to that of regular cells, with distinguishable vacuoles and other organelles. SEM was used to further visualize the external appearance of microcells and shed capsule and clearly demonstrated that these were distinct structures (Fig. S1E to G).

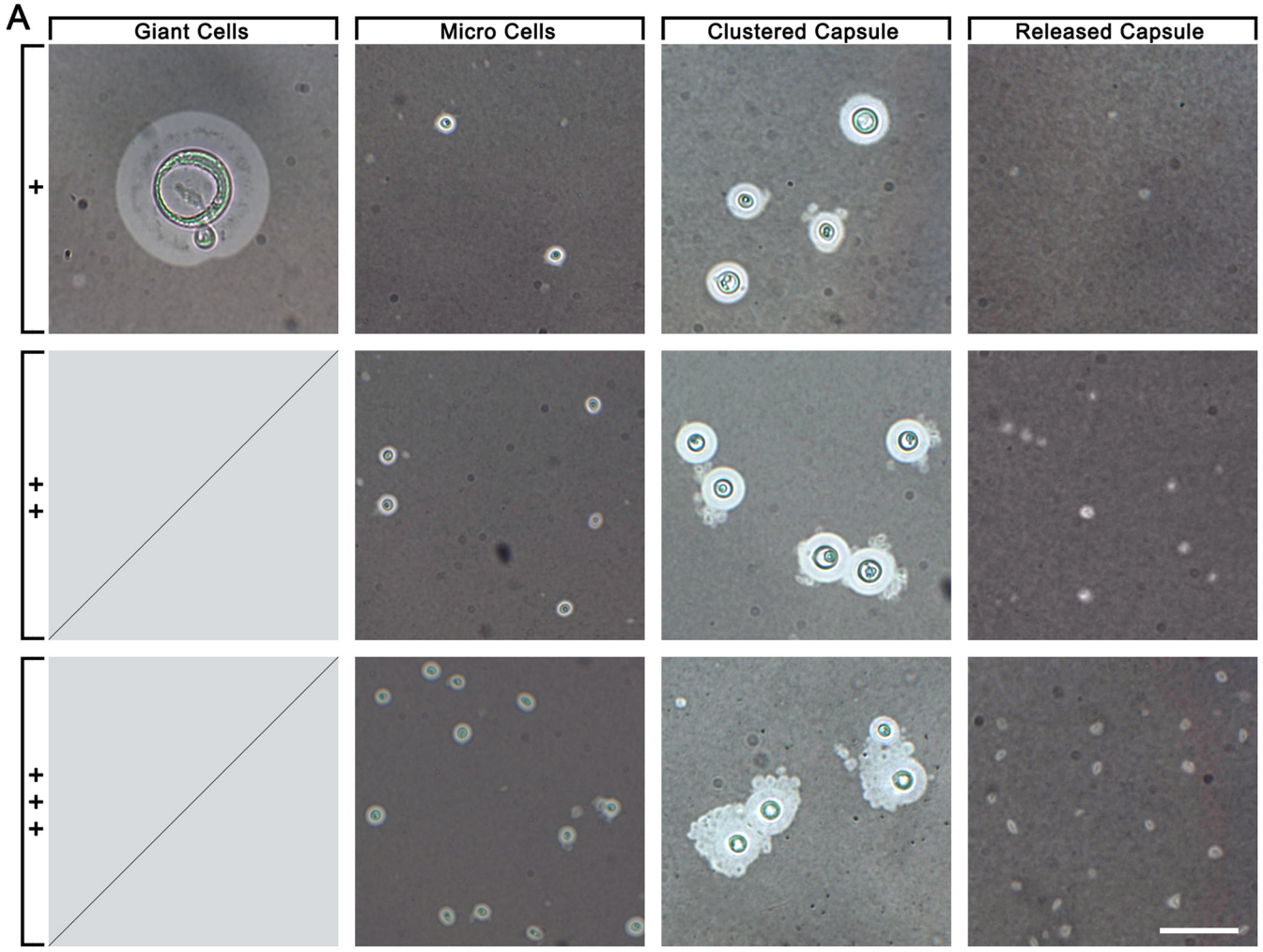

B

	Less Virulent			Intermediate	Hypervirulent				
	H99C	H99E	H99W	H99O	H99S	H99L	KN99a	KN99α	H99F
Giant Cells	–	+	–	+	–	–	–	–	–
Micro Cells	–	–	–	+	+	+	+ + +	+ + +	+ +
Released Capsule	–	+	+	+	+ +	+ +	+ + +	+ + +	+ +
Clustered Capsule	+	–	+	+	+ + +	+ + +	+	+ +	+ + +

FIG 3 Hypervirulent H99 strains produce morphological variants at a much higher frequency than intermediate and less virulent strains following growth under capsule-inducing conditions. (A) India ink preparations of H99 strains showing morphological variants produced following growth in DMEM with 5% CO_2 at 37°C for 5 days, including giant cells larger than 10 μm, microcells smaller than 2 μm, extracellular capsule clustered around cells (clustered capsule), and extracellular capsule released into the media (released capsule). Scoring on the left shows the approximate relative frequency of morphological variants seen in a typical field of view, as presented in panel B.

Deletion of *SGF29* increases the production of morphological variants in the H99O lineage but not the H99S lineage. Given that a 734-bp deletion in *SGF29* in the H99L lineage has been implicated in the switch to hypervirulence, we investigated the effect of *SGF29* deletion on the production of cell phenotype variants. To do so, we used *SGF29* knockout and complemented strains in the background of a strain with intermediate virulence (H99O) and a strain with hypervirulence independent of the *SGF29* deletion (H99S) described in reference 9, H99O.2 and H99S.2, which were used in the creation of the

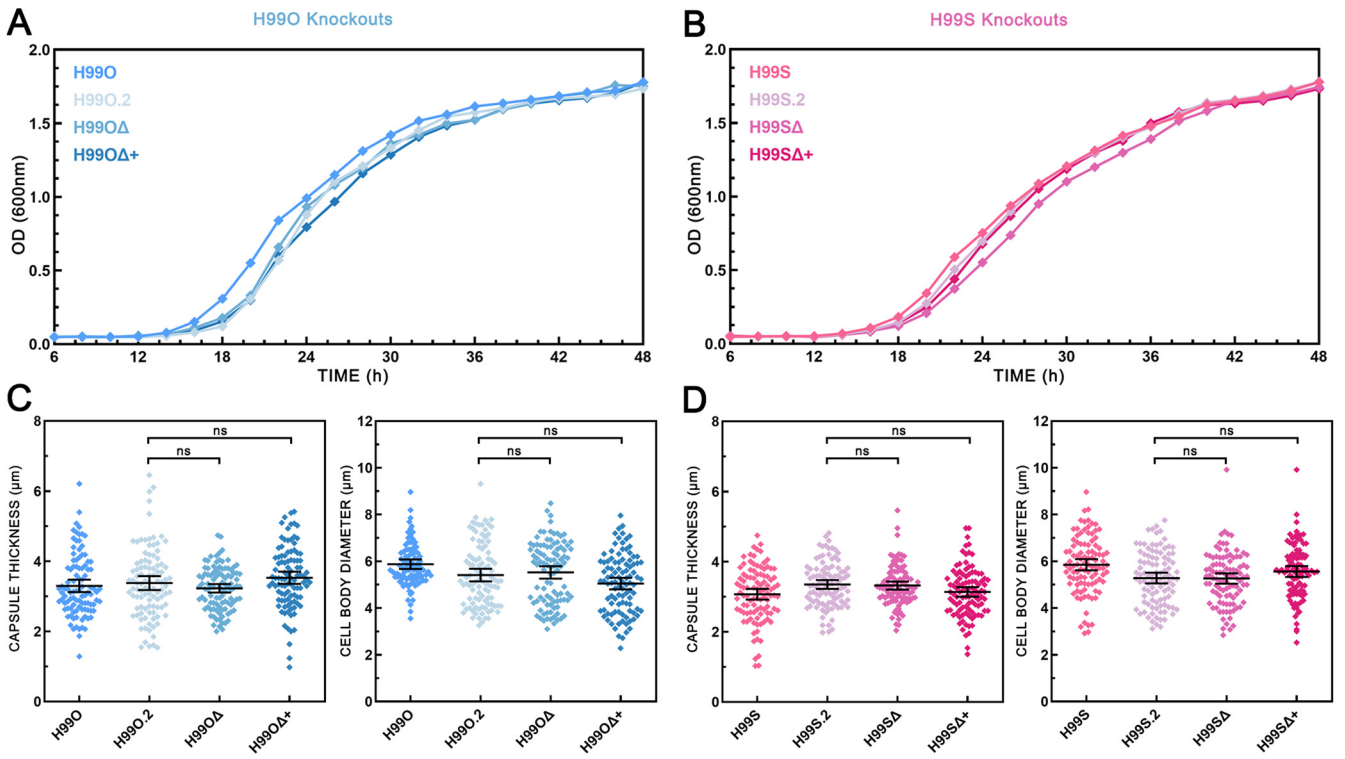

E

	H99O Knockouts			
	H99O	H99O.2	H99OΔ	H99OΔ+
Giant Cells	–	–	–	–
Micro Cells	+	+	+ +	+ +
Released Capsule	+	+	+ +	+ +
Clustered Capsule	+	+	+ +	+ +

F

	H99S Knockouts			
	H99S	H99S.2	H99SΔ	H99SΔ+
Giant Cells	–	–	–	–
Micro Cells	+	+	+	+
Released Capsule	+ +	+ +	+ +	+ +
Clustered Capsule	+	+	+	+

FIG 4 Deletion of *SGF29* increases the production of morphological variants by H99O but not by H99S. Growth curves of wild-type and *sgf29* knockout strains of H99O (A) and H99S (B) incubated at 30°C with 180-rpm shaking averaged across three independent replicates showing no substantial differences among strains. Capsule thickness (left) and cell body diameter (right) of wild-type and *sgf29* knockout strains of H99O (C) and H99S (D) grown in DMEM with 5% CO_2 at 37°C for 5 days. Strains were compared using two-tailed unpaired *t* tests with Welch's correction. Error bars show the means ±95% confidence intervals, $n = 100$. The relative frequency of morphological variants in wild-type and *sgf29* knockout strains of H99O (E) and H99S (F) are shown; see Fig. 3A for scoring process. H99O.2 and H99S.2 are independently sourced and presumed identical copies of H99O and H99S, respectively. H99OΔ = $sgf29\Delta^{H99O}$; H99OΔ+ = *sgf29*Δ + $SGF29^{H99O}$; H99SΔ = $sgf29\Delta^{H99S}$; H99SΔ+ = *sgf29*Δ + $SGF29^{H99S}$.

deletion strains and are presumed to be identical copies of H99O and H99S, respectively; $sgf29\Delta^{H99O}$ (here named H99OΔ) and $sgf29\Delta^{H99S}$ (named H99SΔ), which are *sgf29*Δ deletion mutants created by biolistic transformation; and *sgf29*Δ + $SGF29^{H99O}$ (here named H99OΔ+) and *sgf29*Δ + $SGF29^{H99S}$ (named H99SΔ+), which are *sgf29*Δ deletion mutants complemented with wild-type *SGF29* (9) (Table 1).

Growth curves of wild-type, mutant, and complemented strains under standard growth conditions (SDB at 30°C) over 48 h confirmed that there were no significant differences or abnormalities in the growth rate of these strains (Fig. 4A and B). Antifungal susceptibility testing showed that H99SΔ and H99SΔ+ had 2-fold reduced susceptibility to FLC, ITC, and VRC, while mutant and complement strains of H99O displayed no differences compared to the wild type (Table 1). After growth under capsule-inducing conditions in DMEM with CO_2 at 37°C for 5 days, there were no significant differences in capsule thickness or cell body diameter between H99O.2 and either H99OΔ or H99OΔ+ and between H99S.2 and either H99SΔ or H99SΔ+ (Fig. 4C and D). H99O.2 and H99S.2 produced the same types and amounts of morphological variants as H99O and H99S, indicating that these traits are stable characteristics of the strain. In the

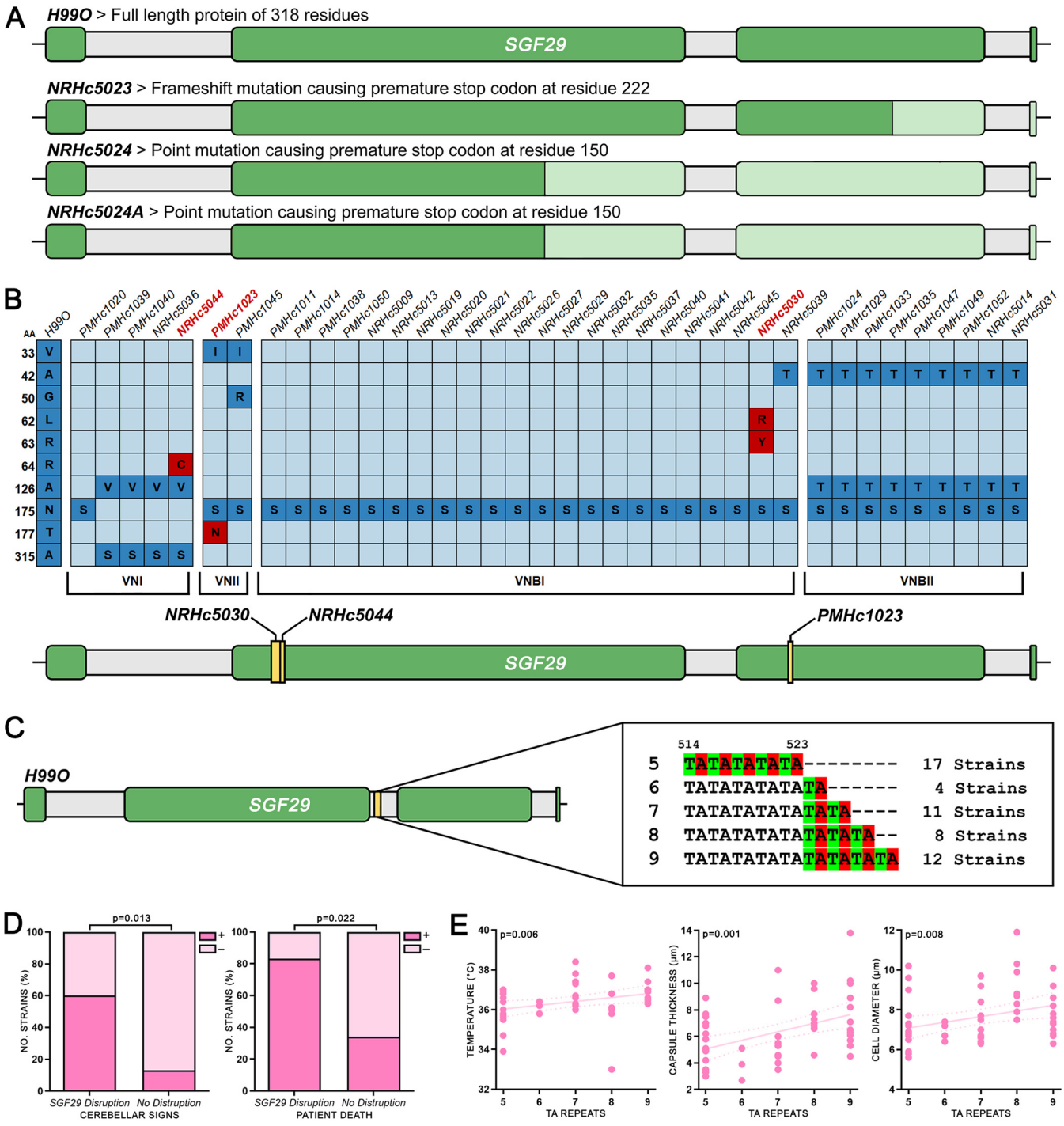

FIG 5 Mutations in *SGF29* in clinical isolates correlate with clinical and phenotypic variables. (A) Strains with mutations occurring in the *SGF29* gene resulting in truncated proteins. Lighter green sections indicate areas of deletion. (B) Strains with missense mutations occurring in the coding regions of the *SGF29* gene (top) and the location of the mutations (bottom). Dark blue boxes indicate mutations predicted to be neutral, while red boxes indicate mutations predicted to be deleterious. (C) Tandem TA repeats ranging from 5 to 9 copies identified in the second intron of *SGF29*. (D) Significant correlations between clinical variables and strains possessing disruptions in *SGF29* (including both mutations resulting in truncated proteins and deleterious missense mutations). (E) Significant correlations between clinical and phenotypic variables and the number of TA repeats in the second intron of *SGF29*.

H99O lineage, the H99OΔ mutant produced substantially increased amounts of microcells, released capsule, and clustered capsule, and this was retained in the complemented H99OΔ+ strain. In contrast, in the H99S lineage, the H99SΔ mutant and its complement strain H99SΔ+ displayed no appreciable difference in the presence or frequency of morphological variants.

In clinical isolates, loss-of-function mutations in *SGF29* correlate with patient death. Based on the association between *sgf29*Δ, virulence, and cell phenotypes seen in the H99 strains, we extended our analysis of *SGF29* to a set of clinical isolates from Botswana that had been fully sequenced and extensively analyzed for cell morphology and associations with clinical parameters (5). Using whole-genome sequencing data (19) (accession numbers are in Table S1 in the supplemental material), we examined *SGF29* in 52 *C. neoformans* strains across 4 genotypes (VNI, $n = 16$; VNII, $n = 2$; VNBI, $n = 25$; VNBII, $n = 9$). Three strains, NRHc5023, NRHc5024, and NRHc5024A (all VNBI strains), were identified with truncated Sgf29 proteins as a result of either frameshift or point mutations resulting in premature stop codons (Fig. 5A). An additional three strains, NRHc5044 (VNI), PMHc1023 (VNII), and NRHc5030 (VNBI), were identified with missense mutations within the coding region of *SGF29* that were predicted to be deleterious by the online tools PROVEAN and PolyPhen-2 (Fig. 5B). In addition, tandem TA repeats ranging from 5 to 9 copies were identified in the second intron of *SGF29* (Fig. 5C and Table S1). The number of repeats was significantly greater in VNBI, previously found to be the most genetically diverse and the most virulent genotype, than in all other genotypes ($P < 0.001$) (5).

Correlations were assessed between either loss-of-function mutations or TA repeat number and the clinical and phenotypic variables recorded for these strains. Significant correlations were found between loss-of-function mutations, cerebellar signs ($P = 0.013$), and patient death ($P = 0.022$), indicating that Sgf29 disruption affects hypervirulence in clinical isolates (Fig. 5D). Additionally, of these six strains, five produced microcells and shed capsule at high frequencies that were comparable to the hypervirulent H99 strains, while only one produced giant cells and none produced irregular cells. For the TA repeat, significant correlations were found between more TA units and higher patient temperature ($P = 0.006$) as well as greater capsule ($P = 0.001$) and cell body ($P = 0.008$) size (Fig. 5E).

DISCUSSION

The capacity to be pleomorphic aligns with virulence. Many studies have sought to correlate individual phenotypes with virulence, the most common being capsule size; however, these attempts have yielded substantially different results. For example, recent studies have reported larger capsules led to greater virulence in zebrafish (20), that smaller capsules resulted in increased macrophage uptake and decreased long-term patient survival (21), and that there was no association between capsule size and virulence in mice (22). Other studies have found strains with increased capsule shedding were associated with higher patient mortality (23) and that neurovirulence may be related to the total amount and speed of accumulation of capsule in the brain rather than the capsule size of individual cells (24). The disparate nature of these results likely reflects the fact that rather than a simple association with a single phenotype driving virulence, it is likely a combination of multiple phenotypes that determines the overall virulence profile of a strain.

In our previous study on Botswanan clinical isolates, we found significant correlations between phenotype and clinical variables, suggesting a relationship between the two, including an association between the production of a range of cell variants and host death (5). However, the heterogenous nature of the data set made determining causation difficult. In the current study, looking at a set of strains with high genetic similarity, we have found the hypervirulent strains to be associated with larger average capsule, increased cell size variation, and increased production of microcells, released capsule, and clustered capsule (Table 1). Taken together, the results of these two studies suggest that, rather than the production of any one phenotype, it is the capacity to be variable and produce a diverse range of phenotypes that is a potential driving factor behind increased virulence. In addition to the individual phenotypes themselves being associated with various routes of pathogenesis, increased morphological heterogeneity as a whole may also contribute to virulence via immune escape.

Most of these variant phenotypes are still largely unexplored, with their presence in samples often not determined or noted but not included in analyses. Microcells, although having been reported as a common feature of cryptococcal infection (4, 17), and irregular cells, although observed in dozens of strains across *C. neoformans* and the *C. gattii* complex (5, 25), remain understudied. This may stem from the fact that most analyses of *Cryptococcus* are done using media that do not provide similar stresses to those encountered during mammalian infection and are therefore unable to induce these phenotypes. Similarly, while giant/titan cell types have become well known in the cryptococcal community, a reliable way of inducing them *in vitro* was only recently developed (13).

Microevolution and epigenetic plasticity enable phenotypic variation. It is well established that many fungal species, including *Cryptococcus*, can readily undergo morphological transitions in response to different environmental stimuli (26). What is less well understood are the exact mechanisms driving this morphogenesis and how it can affect virulence and the progression of disease. Microevolution is a term that typically refers to heritable changes accumulated over a relatively short period of time. The microevolution of cryptococcal strains over the course of infection has been well documented (27–30), an unsurprising fact given that *Cryptococcus* can establish chronic infections that can last months to years, during which the organism is subject to selection by host defense mechanisms (31). While this kind of microevolution often involves changes to the genome, instances of serial isolates displaying strong phenotypic changes with no or very limited genetic changes have also been noted (32). This suggests that epigenetic mechanisms are involved that regulate gene expression and cellular response without altering the DNA sequence.

In the hypervirulent H99L lineage strains, the 734-bp deletion in *SGF29* is thought to play a role in their development of hypervirulence, presumably through the loss of histone H3K9 acetylation altering gene transcription across the genome. Studies looking at epigenetic regulation in *Cryptococcus* have found links between histone deacetylases and a range of cellular functions, including thermotolerance, capsule formation, melanin synthesis, protease activity (33), and drug sensitivity (34); however, relatively little is known about the role of epigenetics in regulating genome plasticity (35). In *Candida*, more direct links have been established, with a recent study observing dynamic heterochromatin remodeling in response to changing the growth temperature from 30°C to 39°C, indicating that differential chromatin states controlling gene expression are linked to rapid adaptation (36).

In the H99OΔ mutant, we found substantially increased production of microcells, released capsule, and clustered capsule, consistent with its switch to the hypervirulent phenotype (Table 1, Fig. 4) (9) and indicating that the loss of *SGF29* was indeed responsible for the enhanced variant production in the H99L lineage. However, this increased production of variants was retained in the complemented H99OΔ+ strain. Although unexpected, this result aligns with the previous finding where the reintroduction of *SGF29* was not sufficient to abolish hypervirulence in H99OΔ (9) and strongly indicates that epigenetic memory, which is difficult to restore, is involved in both the switch to hypervirulence and the production of variant phenotypes. Furthermore, removal and reintroduction of *SGF29* in an H99S background had no appreciable effect on either virulence (9) or morphological variation, and it appears that other mechanisms underlie the increased virulence of this lineage. In contrast to the other hypervirulent strains that are thought to have arisen during routine passaging, H99S acquired hypervirulence during passage through an animal model. This, coupled with the fact that H99S possesses no genetic mutations that can account for its hypervirulence, suggests that it has undergone substantial epigenetic change during its creation that is independent of the SAGA complex.

Also of interest was the observation that hypervirulent strains H99S, H99F, KN99**a**, and KN99α had increased susceptibility to azole drugs (Table 1), indicating a role of Sgf29 in the response to azole antifungals. Azole drugs function through inhibiting

ergosterol synthesis, but while Sgf29 has been observed to alter the expression of ergosterol biosynthesis gene *ERG5* in some strains, it appears to have no effect in others (9). As an epigenetic regulator, the effects of the SAGA complex that includes Sgf29 can be indirect and wide-ranging and, therefore, are difficult to predict. Further study using omics approaches would be very useful for understanding how these strains of variable virulence and phenotype respond to environmental challenges.

Given the apparent association between the loss of Sgf29, virulence, and the presence of morphological variants, we extended our analysis to the clinical isolate set from our previous study on HIV/AIDS patients in Botswana (Fig. 5). Substantial protein truncations and deleterious mutations disrupting *SGF29* were identified in 6 of the 52 clinical strains (11.5%), and the presence of these loss-of-function mutations was found to be significantly correlated with patient death, suggesting hypervirulence. Additionally, a polymorphic TA repeat ranging from 5 to 9 copies was identified in the second intron of *SGF29* in the clinical isolates. Short tandem repeats are common in eukaryotes, including fungi (37). While these mostly occur in noncoding regions and are not predicted to affect phenotype, the presence of self-complementary dinucleotides in introns has been shown to alter gene splicing, presumably through the formation of RNA hairpins, with splicing efficiency inversely correlated with repeat number (38). Here, increasing TA units were found to be significantly correlated with increased patient temperature and greater cell and capsule sizes, indicating a potential link with the regulation and expression of *SGF29*. These findings, together with the previous discovery of *SGF29* loss-of-function mutations in clinical isolates from the United States and India (9), provide further evidence for the importance of Sgf29 in a clinical setting.

The morphological variants observed in this study have distinct cellular properties. Electron microscopy of the cryptococcal cell variant phenotypes revealed new insights into their internal structure. The few giant cells observed here share similarities with titan cells reported in the literature, containing multiple small vesicles per cell and/or a single enlarged vacuole (12, 13). The giant cell shown in Fig. S1A in the supplemental material has a cell wall of 820 nm, which is larger than some reports of titan cells (314.7 $\pm$ 64.0 nm) (13) but smaller than others (2 to 3 μm) (17). These differences may be due to the inducing conditions and not inherent to the cell type itself. SBF-SEM revealed microcells have an internal structure with organelles that seem similar to those seen in regularly sized cells and are distinct from shed capsule. This, together with the fact that their size is outside the range of regular cell sizes, suggests that microcells are a distinct cell type produced by regularly sized cells and are not simply at the small end of a spectrum of regular cell sizes.

Two types of capsule shedding were noted in this study: released capsule that was present in the medium and clustered capsule that appeared to be attached to otherwise regular cells (Fig. 3). There is currently little known about the capsular release mechanism of *Cryptococcus* and whether it is an active phenomenon or merely nonspecific shedding (39), although some studies indicate that capsular and exopolysaccharide materials originate from different pools (40). Some of the clustered capsules observed by light microscopy (Fig. 3A) appeared to have very small amounts of material contained within it that might be picked up inside the cell or pinched off as it exited the cell, implying an active phenomenon. However, in other cases capsule clusters appeared to have burst from the outer capsule, and it is quite possible that there are multiple capsule release mechanisms that have yet to be elucidated.

In our prior study of Botswanan clinical isolates, we found irregular cells with elongated cell morphologies to be significantly more likely to occur in isolates obtained from patients who had undergone antifungal therapy prior to admission. Their presence was also negatively correlated with patient death, suggesting they either are defective cells or a form of persister cell able to establish a chronic but nonlethal infection (5). Here, we observed them to have substantially thinner cell walls than even microcells (Fig. S1), which supports the idea that they may be more fragile and possibly defective. These cells share properties similar to those of a recently described group of cells, termed titanides, characterized by a smaller cell size (2 to 4 μm), oval shape, and

thinner cell walls. However, while titanides appear to be derived from titan cells, this is unlikely for the irregular cells observed here, as they were present in samples that did not contain giant cells (13). Irregular cells were produced most frequently by the hypervirulent congenic strain pair KN99**a** and KN99α, which displayed increased susceptibility to azole drugs and also produced the highest levels of other morphological variants. This raises the question of whether this phenotype is a consequence of the cell machinery producing large numbers of variants. More research into the exact nature of irregular cells will help us understand whether they are a phenotype of benefit to the cell or a defective by-product of phenotypic transition.

Conclusions. Using a set of genetically similar but phenotypically diverse strains, we have shown a potential link between the capacity for phenotypic plasticity and virulence. We have provided further evidence that Sgf29 is an important epigenetic regulator that is likely involved in the transition to a hypervirulent phenotype and have shown that loss-of-function mutations in *SGF29* are also linked to virulence in clinical strains. Other pathways to increased virulence and pleomorphism also occur, however, as demonstrated with H99S. Together, our results demonstrate an impressive ability of *Cryptococcus* to produce variation even when growing as a clonal lineage, which may account for its capacity to produce a persistent, chronic infection in mammalian hosts.

MATERIALS AND METHODS

Test strains. A collection of nine derivatives of *C. neoformans* strain H99 (8, 10) were used in this study, with details in Fig. 1 and Table 1. *SGF29* mutant strains described in reference 9 were also used, with details in Table 1. Botswanan clinical isolates described in reference 5 were used for bioinformatic analysis, with details in Table S1 in the supplemental material.

Growth curves and capsule induction. Culture conditions were as described in reference 5. Before experiments, cells were collected from overnight cultures by centrifugation and washed once with phosphate-buffered saline (PBS). For growth curves, 10^3 cells were inoculated into 2.5 mL of Sabouraud dextrose broth (SDB) in a 12-well tissue culture plate. Plates were incubated at 30°C with 180-rpm shaking, and cell density was measured every 2 h by absorbance at 600 nm for a total of 48 h. For capsule induction, 10^5 cells were inoculated into 5 mL of Dulbecco's modified Eagle medium (DMEM; Life Technologies) in a 6-well tissue culture plate and incubated with 5% CO_2 at 37°C for 5 days.

Staining and microscopy. Staining, microscopy, and measurements of cell and capsule size were performed as described in reference 5, with slight modifications. Cells with yeast cell body greater than 10 μm or less than 2 μm were identified as giant cells or microcells, respectively. Giant cells, microcells, and irregular cells along with extracellular capsule were classified as morphological variants and were enumerated independently. For each strain, the relative frequency of microcells, giant cells, released extracellular capsule, and clustered extracellular capsule was determined by looking over 20 random fields of view containing a minimum of 100 regular cells in total at $\times$40 magnification, and a category was assigned denoting either absence (**–**) or presence at one of three relative frequency levels (**+, ++, or +++**). Irregular cells were calculated as a percentage of the regular cell population, including at least 100 cells.

***Galleria mellonella* infection assays.** *G. mellonella* infection assays were performed as described in reference 41. Briefly, for each test group, 10 larvae were injected with an inoculum of 10^8 cells, placed into a clean petri dish, and incubated at 35°C. The survival or death of each larva was recorded at 24-h intervals over a period of 10 days.

Antifungal susceptibility assays. Antifungal susceptibility assays were performed as described in reference 41 and in accordance with CLSI guideline M27-A3 for yeasts (42). Drugs were assayed at concentration ranges of 0.0039 to 4 μg/mL for AMB, NYS, ITC, and VRC and 0.0625 to 64 μg/mL for FLC and 5FC. Plates were incubated without agitation at 35°C for 72 h.

SEM. For standard scanning electron microscopy (SEM), sample preparation and visualization were performed as described in reference 41. For SBF-SEM, a single block was produced for analysis by mixing together aliquots from strains known to produce appreciable numbers of the different cell phenotypes (H99E, H99W, H99O, H99S, and KN99**a**) following capsule induction. Cells were harvested and washed with 0.1 M phosphate buffer (PB), covered with 1 mL of fixative (2.5% glutaraldehyde, 2% paraformaldehyde, 0.1 M PB), and left overnight at 4°C. Secondary fixation, staining, ethanol dehydration, resin infiltration, and embedding were performed as described in reference 18. The final sample block contained approximately 5,000 cells. The sample block was then loaded onto a Zeiss Sigma variable-pressure SEM equipped with Gatan 3View 2XP. Inverted backscattered electron images (8,192 by 8,192 pixels, 16-bit) were acquired with an *xy* pixel size of 100 nm and *z* pixel size (slice thickness) of 10 nm.

Bioinformatic analysis of clinical isolates. Sequencing data were downloaded from the NCBI Sequence Read Archive and assembled and analyzed using Geneious 6.0.6. The effect of missense mutations on the functionality of the protein was predicted using the PROVEAN (43) and PolyPhen-2 (44) online tools and validated with assistance from the PRALINE tool (45) to confirm changes to hydrophobicity.

Statistical analysis. Significant differences between treatment groups for *Galleria* infection assays were determined using the log rank test to compare the distributions between each pair of strains. Significant differences between strains for phenotypic data were determined using two-tailed unpaired *t* tests with Welch's correction, and differences in variance were assessed by F test analysis. For correlations between genetic, clinical, and phenotypic data, tests between continuous variables used Spearman rank-order correlations, those between continuous and binary variables used Mann-Whitney U tests, and those between binary variables used chi-square tests or Fisher's exact tests if any expected value was <5. *P* values of <0.05 were considered significant. Error bars represent the means $\pm$95% confidence intervals. Data were analyzed using Excel (Microsoft Corporation), Prism 5 (GraphPad Inc.), and SPSS Statistics (IBM) software.

SUPPLEMENTAL MATERIAL

Supplemental material is available online only.

FIG S1, JPG file, 0.9 MB.

TABLE S1, XLSX file, 0.02 MB.

ACKNOWLEDGMENTS

We acknowledge the facilities as well as the scientific and technical assistance of the Microscopy Australia (micro.org.au) node at the University of Sydney: Sydney Microscopy & Microanalysis. We thank Christina Cuomo and Poppy Sephton-Clark (Broad Institute) for their assistance with genomic data analysis.

K.E.F. and D.A.C. conceived and designed the experiments. K.E.F. produced, collated, and analyzed the data and wrote the manuscript with assistance from D.A.C. and J.A.F.

REFERENCES

1. Perfect JR, Bicanic T. 2015. Cryptococcosis diagnosis and treatment: what do we know now. Fungal Genet Biol 78:49–54. https://doi.org/10.1016/j.fgb.2014.10.003.
2. Rajasingham R, Smith RM, Park BJ, Jarvis JN, Govender NP, Chiller TM, Denning DW, Loyse A, Boulware DR. 2017. Global burden of disease of HIV-associated cryptococcal meningitis: an updated analysis. Lancet Infect Dis 17:873–881. https://doi.org/10.1016/S1473-3099(17)30243-8.
3. Krysan DJ. 2017. The unmet clinical need of novel antifungal drugs. Virulence 8:135–137. https://doi.org/10.1080/21505594.2016.1276692.
4. Zaragoza O. 2011. Multiple disguises for the same party: the concepts of morphogenesis and phenotypic variations in *Cryptococcus neoformans*. Front Microbiol 2:181. https://doi.org/10.3389/fmicb.2011.00181.
5. Fernandes KE, Brockway A, Haverkamp M, Carter DA, Cuomo CA, van Ogtrop F, Perfect JR. 2018. Phenotypic variability correlates with clinical outcome in *Cryptococcus* isolates obtained from Botswanan HIV/AIDS patients. mBio 9:e02016-18. https://doi.org/10.1128/mBio.02016-18.
6. Altamirano S, Jackson KM, Nielsen K. 2020. The interplay of phenotype and genotype in *Cryptococcus neoformans* disease. Biosci Rep 40:e0337. https://doi.org/10.1042/BSR20190337.
7. Zafar H, Altamirano S, Ballou ER, Nielsen K. 2019. A titanic drug resistance threat in *Cryptococcus neoformans*. Curr Opin Microbiol 52:158–164. https://doi.org/10.1016/j.mib.2019.11.001.
8. Janbon G, Ormerod KL, Paulet D, Byrnes EJ, Yadav V, Chatterjee G, Mullapudi N, Hon CC, Billmyre RB, Brunel F, Bahn YS, Chen W, Chen Y, Chow EWL, Coppée JY, Floyd-Averette A, Gaillardin C, Gerik KJ, Goldberg J, Gonzalez-Hilarion S, Gujja S, Hamlin JL, Hsueh YP, Ianiri G, Jones S, Kodira CD, Kozubowski L, Lam W, Marra M, Mesner LD, Mieczkowski PA, Moyrand F, Nielsen K, Proux C, Rossignol T, Schein JE, Sun S, Wollschlaeger C, Wood IA, Zeng Q, Neuvéglise C, Newlon CS, Perfect JR, Lodge JK, Idnurm A, Stajich JE, Kronstad JW, Sanyal K, Heitman J, Fraser JA, Cuomo CA, et al. 2014. Analysis of the genome and transcriptome of *Cryptococcus neoformans* var. *grubii* reveals complex RNA expression and microevolution leading to virulence attenuation. PLoS Genet 10:e1004261. https://doi.org/10.1371/journal.pgen.1004261.
9. Arras SDM, Ormerod KL, Erpf PE, Espinosa MI, Carpenter AC, Blundell RD, Stowasser SR, Schulz BL, Tanurdzic M, Fraser JA. 2017. Convergent microevolution of *Cryptococcus neoformans* hypervirulence in the laboratory and the clinic. Sci Rep 7:17918. https://doi.org/10.1038/s41598-017-18106-2.
10. Nielsen K, Cox GM, Wang P, Toffaletti DL, Perfect JR, Heitman J. 2003. Sexual cycle of *Cryptococcus neoformans* var. *grubii* and virulence of congenic a and α isolates. Infect Immun 71:4831–4841. https://doi.org/10.1128/IAI.71.9.4831-4841.2003.
11. Dyląg M, Colon-Reyes RJ, Kozubowski L. 2020. Titan cell formation is unique to *Cryptococcus* species complex. Virulence 11:719–729. https://doi.org/10.1080/21505594.2020.1772657.
12. Okagaki LH, Strain AK, Nielsen JN, Charlier C, Baltes NJ, Chrétien F, Heitman JH, Dromer F, Nielsen KN. 2010. Cryptococcal cell morphology affects host cell interactions and pathogenicity. PLoS Pathog 6:e1000953. https://doi.org/10.1371/journal.ppat.1000953.
13. Dambuza IM, Drake T, Chapuis A, Zhou X, Correia J, Taylor-Smith L, LeGrave N, Rasmussen T, Fisher MC, Bicanic T, Harrison TS, Jaspars M, May RC, Brown GD, Yuecel R, MacCallum DM, Ballou ER. 2018. The *Cryptococcus neoformans* titan cell is an inducible and regulated morphotype underlying pathogenesis. PLoS Pathog 14:e1006978. https://doi.org/10.1371/journal.ppat.1006978.
14. Hommel B, Mukaremera L, Cordero RJB, Coelho C, Desjardins CA, Sturny-Leclère A, Janbon G, Perfect JR, Fraser JA, Casadevall A, Cuomo CA, Dromer F, Nielsen K, Alanio A. 2018. Titan cells formation in *Cryptococcus neoformans* is finely tuned by environmental conditions and modulated by positive and negative genetic regulators. PLoS Pathog 14:e1006982. https://doi.org/10.1371/journal.ppat.1006982.
15. Zaragoza O, Nielsen K. 2013. Titan cells in *Cryptococcus neoformans*: cells with a giant impact. Curr Opin Microbiol 16:409–413. https://doi.org/10.1016/j.mib.2013.03.006.
16. García-Barbazán I, Trevijano-Contador N, Rueda C, de Andrés B, Pérez-Tavárez R, Herrero-Fernández I, Gaspar ML, Zaragoza O. 2016. The formation of titan cells in *Cryptococcus neoformans* depends on the mouse strain and correlates with induction of Th2-type responses. Cell Microbiol 18:111–124. https://doi.org/10.1111/cmi.12488.
17. Feldmesser M, Kress Y, Casadevall A. 2001. Dynamic changes in the morphology of *Cryptococcus neoformans* during murine pulmonary infection. Microbiology (Reading) 147:2355–2365. https://doi.org/10.1099/00221287-147-8-2355.
18. Shami GJ, Cheng D, Braet F. 2018. Silver filler pre-embedding to enhance resolution and contrast in multidimensional SEM: a nanoscale imaging study on liver tissue. Methods Mol Biol 1814:561–576. https://doi.org/10.1007/978-1-4939-8591-3_33.
19. Desjardins CA, Giamberardino C, Sykes SM, Yu CH, Tenor JL, Chen Y, Yang T, Jones AM, Sun S, Haverkamp MR, Heitman J, Litvintseva AP, Perfect JR, Cuomo CA. 2017. Population genomics and the evolution of virulence in the fungal pathogen *Cryptococcus neoformans*. Genome Res 27:1207–1219. https://doi.org/10.1101/gr.218727.116.

20. Bojarczuk A, Miller KA, Hotham R, Lewis A, Ogryzko NV, Kamuyango AA, Frost H, Gibson RH, Stillman E, May RC, Renshaw SA, Johnston SA. 2016. *Cryptococcus neoformans* intracellular proliferation and capsule size determines early macrophage control of infection. Sci Rep 6:21489. https://doi.org/10.1038/srep21489.
21. Sabiiti W, Robertson E, Beale MA, Johnston SA, Brouwer AE, Loyse A, Jarvis JN, Gilbert AS, Fisher MC, Harrison TS, May RC, Bicanic T. 2014. Efficient phagocytosis and laccase activity affect the outcome of HIV-associated cryptococcosis. J Clin Invest 124:2000–2008. https://doi.org/10.1172/JCI72950.
22. Mukaremera L, Mcdonald TR, Nielsen JN, Molenaar CJ, Akampurira A, Schutz C, Taseera K, Muzoora C, Meintjes G, Meya DB, Boulware DR, Nielsen K. 2019. The mouse inhalation model of *Cryptococcus neoformans* infection recapitulates strain virulence in humans and shows that closely related strains can possess differential virulence. Infect Immun 87:e00046-19. https://doi.org/10.1128/IAI.00046-19.
23. Wiesner DL, Moskalenko O, Corcoran JM, Mcdonald T, Rolfes MA, Meya DB, Kajumbula H, Kambugu A, Bohjanen PR, Knight JF, Boulware DR, Nielsen K. 2012. Cryptococcal genotype influences immunologic response and human clinical outcome after meningitis. mBio 3:e00196-12. https://doi.org/10.1128/mBio.00196-12.
24. Pool A, Lowder L, Wu Y, Forrester K, Rumbaugh J. 2013. Neurovirulence of *Cryptococcus neoformans* determined by time course of capsule accumulation and total volume of capsule in the brain. J Neurovirol 19:228–238. https://doi.org/10.1007/s13365-013-0169-7.
25. Fernandes KE, Dwyer C, Campbell LT, Carter DA. 2016. Species in the *Cryptococcus gattii* complex differ in capsule and cell size following growth under capsule-inducing conditions. mSphere 1:e00350-16. https://doi.org/10.1128/mSphere.00350-16.
26. Fernandes KE, Carter DA. 2020. Cellular plasticity of pathogenic fungi during infection. PLoS Pathog 16:e1008571. https://doi.org/10.1371/journal.ppat.1008571.
27. Fries BC, Casadevall A. 1998. Serial isolates of *Cryptococcus neoformans* from patients with AIDS differ in virulence for mice. J Infect Dis 178:1761–1766. https://doi.org/10.1086/314521.
28. Ormerod KL, Morrow CA, Chow EWL, Lee IR, Arras SDM, Schirra HJ, Cox GM, Fries BC, Fraser JA. 2013. Comparative genomics of serial isolates of *Cryptococcus neoformans* reveals gene associated with carbon utilization and virulence. G3. G3 (Bethesda) 3:675–686. https://doi.org/10.1534/g3.113.005660.
29. Hu G, Chen SH, Qiu J, Bennett JE, Myers TG, Williamson PR. 2014. Microevolution during serial mouse passage demonstrates *FRE3* as a virulence adaptation gene in *Cryptococcus neoformans*. mBio 5:e00941-14. https://doi.org/10.1128/mBio.00941-14.
30. Blasi E, Brozzetti A, Francisci D, Neglia R, Cardinali G, Bistoni F, Vidotto V, Baldelli F. 2001. Evidence of microevolution in a clinical case of recurrent *Cryptococcus neoformans* meningoencephalitis. Eur J Clin Microbiol Infect Dis 20:535–543. https://doi.org/10.1007/s100960100549.
31. Casadevall A, Coelho C, Cordero RJB, Dragotakes Q, Jung E, Vij R, Wear MP. 2019. The capsule of *Cryptococcus neoformans*. Virulence 10:822–831. https://doi.org/10.1080/21505594.2018.1431087.
32. Chen Y, Farrer RA, Giamberardino C, Sakthikumar S, Jones A, Yang T, Tenor JL, Wagih O, van Wyk M, Govender NP, Mitchell TG, Litvintseva AP, Cuomo CA, Perfect JR. 2017. Microevolution of serial clinical isolates of *Cryptococcus neoformans* var. *grubii* and *C. gattii*. mBio 8:e00166-17. https://doi.org/10.1128/mBio.00166-17.
33. Brandão F, Esher SK, Ost KS, Pianalto K, Nichols CB, Fernandes L, Bocca AL, Poças-Fonseca MJ, Alspaugh JA. 2018. *HDAC* genes play distinct and redundant roles in *Cryptococcus neoformans* virulence. Sci Rep 8:5209. https://doi.org/10.1038/s41598-018-21965-y.
34. Ranjan K, Brandão F, Morais JAV, Muehlmann LA, Silva-Pereira I, Bocca AL, Matos LF, Poças-Fonseca MJ. 2021. The role of *Cryptococcus neoformans* histone deacetylase genes in the response to antifungal drugs, epigenetic modulators and to photodynamic therapy mediated by an aluminium phthalocyanine chloride nanoemulsion *in vitro*. J Photochem Photobiol B Biol 216:112131. https://doi.org/10.1016/j.jphotobiol.2021.112131.
35. Buscaino A. 2019. Chromatin-mediated regulation of genome plasticity in human fungal pathogens. Genes 10:855. https://doi.org/10.3390/genes10110855.
36. Freire-Benéitez V, Price RJ, Tarrant D, Berman J, Buscaino A. 2016. *Candida albicans* repetitive elements display epigenetic diversity and plasticity. Sci Rep 6:22989. https://doi.org/10.1038/srep22989.
37. Lim S, Notley-McRobb L, Lim M, Carter DA. 2004. A comparison of the nature and abundance of microsatellites in 14 fungal genomes. Fungal Genet Biol 41:1025–1036. https://doi.org/10.1016/j.fgb.2004.08.004.
38. Hefferon TW, Groman JD, Yurk CE, Cutting GR. 2004. A variable dinucleotide repeat in the *CFTR* gene contributes to phenotype diversity by forming RNA secondary structures that alter splicing. Proc Natl Acad Sci U S A 101:3504–3509. https://doi.org/10.1073/pnas.0400182101.
39. Zaragoza O, Rodrigues ML, de Jesus M, Frases S, Dadachova E, Casadevall A. 2009. The capsule of the fungal pathogen *Cryptococcus neoformans*. Adv Appl Microbiol 68:133–216. https://doi.org/10.1016/S0065-2164(09)01204-0.
40. Frases S, Nimrichter L, Viana NB, Nakouzi A, Casadevall A. 2008. *Cryptococcus neoformans* capsular polysaccharide and exopolysaccharide fractions manifest physical, chemical, and antigenic differences. Eukaryot Cell 7:319–327. https://doi.org/10.1128/EC.00378-07.
41. Fernandes KE, Weeks K, Carter DA. 2020. Lactoferrin is broadly active against yeasts and highly synergistic with amphotericin B. Antimicrob Agents Chemother 64:e02284-19. https://doi.org/10.1128/AAC.02284-19.
42. Clinical and Laboratory Standards Institute (CLSI). 2008. Antifungal susceptibility testing–yeasts. Clinical and Laboratory Standards Institute, Wayne, PA.
43. Choi Y, Chan AP. 2015. PROVEAN web server: a tool to predict the functional effect of amino acid substitutions and indels. Bioinformatics 31:2745–2747. https://doi.org/10.1093/bioinformatics/btv195.
44. Adzhubei IA, Schmidt S, Peshkin L, Ramensky VE, Gerasimova A, Bork P, Kondrashov AS, Sunyaev SR. 2010. A method and server for predicting damaging missense mutations. Nat Methods 7:248–249. https://doi.org/10.1038/nmeth0410-248.
45. Simossis VA, Heringa J. 2005. PRALINE: a multiple sequence alignment toolbox that integrates homology-extended and secondary structure information. Nucleic Acids Res 33:W289–W294. https://doi.org/10.1093/nar/gki390.